

# Analytical approach on linear and nonlinear pulse propagations in an open $\Lambda$ -type molecular system with Doppler broadening

Chaohua Tan, Chengjie Zhu and Guoxiang Huang<sup>1</sup>

State Key Laboratory of Precision Spectroscopy and Department of Physics, East China Normal University, Shanghai 200062, China

E-mail: gxhuang@phy.ecnu.edu.cn

**Abstract.** We develop a systematic analytical approach on linear and nonlinear pulse propagations in an open  $\Lambda$ -type molecular system with Doppler broadening. In linear case, by using residue theorem and a spectrum decomposition method, we prove that there exists a crossover from electromagnetically induced transparency (EIT) to Autler-Townes splitting (ATS) for co-propagating configuration of probe and control fields. However, there is no EIT and hence no EIT-ATS crossover for counter-propagating configuration. We give various explicit formulas, including probe-field spectrum decomposition, EIT condition, width of EIT transparency window, as well as a comparison with the result of cold molecules. Our analytical result agrees well with the experimental one reported recently by A. Lazoudis *et al.* [*Phys. Rev. A* **82**, 023812 (2010)]. In nonlinear case, by using the method of multiple-scales, we derive a nonlinear envelope equation for probe-field propagation. We show that stable ultraslow solitons can be realized in the open molecular system.

PACS numbers: 33.40.+f, 42.50.Hz, 42.65.Tg

Submitted to: *J. Phys. B: At. Mol. Opt. Phys.*

## 1. INTRODUCTION

In recent years, much attention has been paid to the study of quantum coherent phenomena in various multi-level systems, typical examples include Auter-Townes splitting (ATS) [1] and electromagnetically induced transparency (EIT) [2]. Such phenomena are not only important from viewpoint of basic research, but also very attractive for many practical applications, such as lasing without inversion, coherent population transfer, enhanced Kerr nonlinearity, slow light, quantum memory, atom and/or photon entanglement, precision spectroscopy, precision measurement, and so on [2, 3].

ATS occurs when absorption spectrum of a quantum transition can be decomposed into a sum of two net Lorentzian terms if one of two levels involved in the transition is coupled to a third level induced by a strong control field. EIT occurs when the absorption spectrum can be decomposed not only into two Lorentzians, but also with additional quantum *destructive* interference term(s). Usually, in systems with ATS or EIT, a transparency window is opened. However, the opening of the transparency window cannot be tell us whether the phenomenon belongs to ATS or EIT, each of which has different physical origin. ATS happens only for strong control field, but EIT happens even the control field is weak. Especially, Only for weak control field can essential characters of EIT be illustrated clearly [4, 5, 6, 7].

EIT in various atomic systems has been studied intensively both theoretically and experimentally [2, 3]. However, systematic investigations of EIT in molecular systems are still lacking. Up to now, there are only several related experimental studies in molecular systems, including the EIT in  ${}^7\text{Li}_2$  [8],  $\text{K}_2$  [10] and  $\text{Na}_2$  vapors [11, 12], in acetylene molecules filled in hollow-core photonic crystal fibers [13, 14] and in photonic microcells [15], and in  $\text{Cs}_2$  in a vapor cell [16], and so on. Major difficulties for observing EIT in molecules are small transition-dipole-moment matrix elements in comparison with those in atoms, and many decay pathways to other molecular states not involved in the main excitation scheme.

In an interesting work reported recently by Lazoudis *et al.* [9], EIT in an open hot  $\Lambda$ -type molecular  ${}^7\text{Li}_2$  system has been studied experimentally. A numerical simulation under steady-state approximation is used by the authors for solving density matrix equations for molecules. Though the numerical simulation is helpful to explain experimental data, it is however hard to discern ATS from EIT objectively because the physical mechanism behind numerical results are not clear. In particular, since open molecular systems with Doppler broadening are very complicated and have very different features in different parameter regions, it is necessary to clarify in an analytical way the quantum interference characters inherent in such systems, which, to the best of our knowledge, has not been done in literature up to now. In addition, it is also necessary to go beyond steady-state approximation if probe pulse is used in experiment.

In this work, we develop a systematic analytical approach on linear and nonlinear pulse propagations in open  $\Lambda$ -type molecular systems with Doppler broadening. In

linear case, by using residue theorem and spectrum decomposition method, we prove clearly that there exists a crossover EIT to ATS for co-propagating configuration of probe and control fields. However, there is no EIT and hence no EIT-ATS crossover for counter-propagating configuration. We provide various explicit formulas, including probe-spectrum decomposition, EIT condition, and width of EIT transparency window, as well as a comparison with the result of cold molecules. Our analytical result agrees well with the experimental one reported recently by A. Lazoudis *et al.* [9]. In nonlinear case, by using a standard method of multiple-scales, we derive a nonlinear envelope equation for probe-field propagation. We show that a stable ultraslow solitons can be realized in the open molecular system. Notice that nonlinear pulse propagation in coherent atomic systems via EIT has attracted tremendous attention in recent years [17, 18, 19, 20, 21, 22, 23, 24], nobody however has considered similar problem for molecules till now.

The article is arranged as follows. In the next section we present our model and associated Maxwell-Bloch (MB) equations. In section 3, we consider the linear property of the system by using residue theorem and spectrum decomposition method. Quantum interference characters for hot molecules with both co- and counter-propagating configurations and also for cold molecules are analyzed in detail. In section 4, the method of multiple-scales is used to study the weak nonlinear propagation of the probe field. Lastly, section 5 contains a summary of the main results obtained in our work.

## 2. Model

The model adopted here is the same as that used in [9]. An open three-state  $\Lambda$ -type  $\text{Li}_2$  molecular system (figure 1) consists of an excited upper-level  $A^1\Sigma_u^+(v' = 5, J' = 13)$  (labeled  $|3\rangle$ ) and two ground states  $X^1\Sigma_g^+(v'' = 1, J'' = 14)$  (labeled  $|1\rangle$ ) and  $X^1\Sigma_g^+(v'' = 0, J'' = 12)$  (labeled  $|2\rangle$ ). A control field with center frequency  $\omega_c$  couples to the excited state  $|3\rangle$  and the ground state  $|2\rangle$ . The other ground state  $|1\rangle$  couples to the  $|3\rangle$  by a probe field with center frequency  $\omega_p$ . The excited level  $|3\rangle$  decay spontaneously to the ground states  $|1\rangle$  and  $|2\rangle$  with decay rates  $\Gamma_{13}$  and  $\Gamma_{23}$ , respectively. The parameter  $\gamma$  represents the transient relaxation rate of the molecule entering and leaving interaction region between light and the molecule. It reflects also the additional relaxation of each state due to the interaction with thermal reservoir [9]. The electric field vector of the system is  $\mathbf{E} = \sum_{l=p,c} \mathbf{e}_l \mathcal{E}_l(z, t) e^{i(\mathbf{k}_l \cdot \mathbf{r} - \omega_l t)} + \text{c.c.}$ , where  $\mathbf{e}_l$  ( $\mathbf{k}_l$ ) is the unit polarization vector (wave number) of the electric field component with the envelope  $\mathcal{E}_l$  ( $l = p, c$ ).

As indicated in the last section, decay processes in molecular systems are very complicated in comparison with those of atoms. There exist many decay pathways to other molecular states not involved in the main excitation scheme, and hence the theoretical model considered is necessarily an open one. In the excitation scheme adopted above, molecules occupying the excited level  $|3\rangle$  may follow various relaxation pathways and decay to many lower vibration-rotation levels besides the levels  $|1\rangle$  and  $|2\rangle$ . In our modeling all these levels are represented by the level  $|4\rangle$ . The decay rate  $\Gamma_{43}$

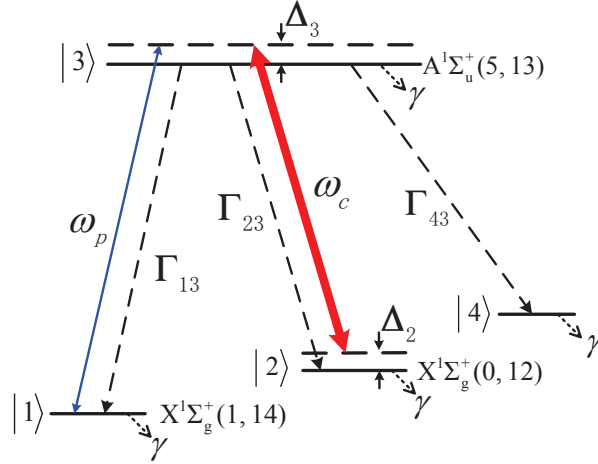


**Figure 1.** (Color online)  $\Lambda$ -type EIT scheme for open  $\text{Li}_2$  molecular system. Excited state  $A^1\Sigma_u^+(v' = 5, J' = 13)$  (labeled |3>) couples to ground state  $X^1\Sigma_g^+(v'' = 0, J'' = 12)$  (labeled |2>) by the control field with center frequency  $\omega_c$  and also to another ground state  $X^1\Sigma_g^+(v'' = 1, J'' = 14)$  (labeled |1>) by the probe field with center frequency  $\omega_p$ .  $\Delta_2$  and  $\Delta_3$  are detunings,  $\Gamma_{jl}$  are population decay rates from  $|l\rangle$  to  $|j\rangle$ , and  $\gamma$  is transit rate. Molecules occupying the excited state |3) may decay to many other states besides the states |1) and |2). All these other states are represented by state |4).

indicates the spontaneous emission rate of level |3) to level |4) (see figure 1).

For hot molecules, inhomogeneous Doppler broadening must be taken into account because the experiments are carried out in a heat-pipe oven [9]. The Hamiltonian of the system in interaction picture under electric-dipole and rotating-wave approximations is

$$\hat{H} = -\hbar(\Omega_c e^{i[\mathbf{k}_c \cdot (\mathbf{r} + \mathbf{v}t) - \omega_c t]} |3\rangle\langle 2| + \Omega_p e^{i[\mathbf{k}_p \cdot (\mathbf{r} + \mathbf{v}t) - \omega_p t]} |3\rangle\langle 1| + \text{c.c.}), \quad (1)$$

where  $\mathbf{v}$  is molecular velocity,  $\Omega_{c(p)} = (\mathbf{e}_{c(p)} \cdot \boldsymbol{\mu}_{32(31)}) \mathcal{E}_{c(p)} / (2\hbar)$  is half Rabi frequency of the control (probe) field, with  $\boldsymbol{\mu}_{jl}$  the electric-dipole matrix element associated with the transition from state  $|j\rangle$  to state  $|l\rangle$ . The optical Bloch equation in the interaction picture reads

$$\begin{aligned} i\frac{\partial}{\partial t}\sigma_{11} + i\gamma(\sigma_{11} - \sigma_{11}^{\text{eq}}) - i\Gamma_{13}\sigma_{33} + \Omega_p^*\sigma_{31} - \Omega_p\sigma_{31}^* &= 0, \\ i\frac{\partial}{\partial t}\sigma_{22} + i\gamma(\sigma_{22} - \sigma_{22}^{\text{eq}}) - i\Gamma_{23}\sigma_{33} + \Omega_c^*\sigma_{32} - \Omega_c\sigma_{32}^* &= 0, \\ i\frac{\partial}{\partial t}\sigma_{33} + i\gamma(\sigma_{33} - \sigma_{33}^{\text{eq}}) + i\Gamma_{33}\sigma_{33} + \Omega_p\sigma_{31}^* + \Omega_c\sigma_{32}^* \\ - \Omega_p^*\sigma_{31} - \Omega_c^*\sigma_{32} &= 0, \\ i\frac{\partial}{\partial t}\sigma_{44} + i\gamma(\sigma_{44} - \sigma_{44}^{\text{eq}}) - i\Gamma_{43}\sigma_{33} &= 0, \\ \left(i\frac{\partial}{\partial t} + d_{21}\right)\sigma_{21} + \Omega_c^*\sigma_{31} - \Omega_p\sigma_{32}^* &= 0, \end{aligned}$$

$$\begin{aligned} \left(i\frac{\partial}{\partial t} + d_{31}\right)\sigma_{31} + \Omega_p(\sigma_{11} - \sigma_{33}) + \Omega_c\sigma_{21} &= 0, \\ \left(i\frac{\partial}{\partial t} + d_{32}\right)\sigma_{32} + \Omega_c(\sigma_{22} - \sigma_{33}) + \Omega_p\sigma_{21}^* &= 0, \end{aligned} \quad (2)$$

for nondiagonal elements, where  $d_{21} = -(\mathbf{k}_p - \mathbf{k}_c) \cdot \mathbf{v} + \Delta_2 - \Delta_1 + i\gamma_{21}$ ,  $d_{31} = -\mathbf{k}_p \cdot \mathbf{v} + \Delta_3 - \Delta_1 + i\gamma_{31}$ ,  $d_{32} = -\mathbf{k}_c \cdot \mathbf{v} + \Delta_3 - \Delta_2 + i\gamma_{32}$  with  $\gamma_{jl} = (\Gamma_j + \Gamma_l)/2 + \gamma + \gamma_{jl}^{\text{col}}$  ( $j, l = 1, 2, 3$ ). Here  $\Delta_j$  ( $j = 1, 2, 3$ ) are detunings, and  $\Gamma_j$  denotes the total decay rate of population out of level  $|j\rangle$ , which is defined by  $\Gamma_j = \sum_{l \neq j} \Gamma_{lj}$ . The quantity  $\gamma_{jl}^{\text{col}}$  is the dephasing rate due to processes such as elastic collisions.  $\sigma_{jj}^{\text{eq}}$  is the thermal equilibrium value of  $\sigma_{jj}$  when all electric-fields are absent. Equation (2) satisfies  $\sum_{j=1}^4 \sigma_{jj} = 1$  with  $\sum_{j=1}^4 \sigma_{jj}^{\text{eq}} = 1$ . At thermal equilibrium, population in the excited state  $|3\rangle$  is much smaller than that of the ground states, i.e.  $\sigma_{33}^{\text{eq}} \simeq 0$  and hence  $\sigma_{11}^{\text{eq}} + \sigma_{22}^{\text{eq}} + \sigma_{44}^{\text{eq}} \simeq 1$ .

The evolution of the electric field is governed by the Maxwell equation. Due to the Doppler effect, the electric polarization intensity of the system is given by  $\mathbf{P} = \mathcal{N}_a \int_{-\infty}^{\infty} dv f(v) \{ \boldsymbol{\mu}_{13} \sigma_{31} \exp[i(k_p z - \omega_p t)] + \boldsymbol{\mu}_{23} \sigma_{32} \exp[i(k_c z - \omega_c t)] + \text{c.c.} \}$ , where  $\mathcal{N}_a$  is molecular density and  $f(v)$  is the molecular velocity distribution function. For simplicity, we have assumed electric-field wavevectors are along  $z$ -direction, i.e.  $\mathbf{k}_{p,c} = (0, 0, k_{p,c})$ . Under the slowly-varying envelope approximation, the Maxwell equation reduces into

$$i \left( \frac{\partial}{\partial z} + \frac{1}{c} \frac{\partial}{\partial t} \right) \Omega_p + \kappa_{13} \int_{-\infty}^{\infty} dv f(v) \sigma_{31}(z, v, t) = 0, \quad (3)$$

with  $\kappa_{13} = \mathcal{N}_a \omega_p |\boldsymbol{\mu}_{31}|^2 / (2\hbar \varepsilon_0 c)$ , here  $c$  is the light speed in vacuum.

The MB equations (2) and (3) are our starting point for the study of linear and nonlinear pulse propagations in the open molecular system with Doppler broadening.

### 3. Linear propagation

#### 3.1. Base state and general linear solution

We first consider linear propagation of the probe field. For this aim, one must know the base state  $\sigma_{jl}^{(0)}$ , i.e. the steady-state solution of the MB equations (2) and (3) for  $\Omega_p = 0$ . It is easy to obtain

$$\begin{aligned} \sigma_{11}^{(0)} &= \frac{[\gamma \Gamma_{3\gamma} X_1 + (2\gamma + \Gamma_{43}) |\Omega_c|^2] \sigma_{11}^{\text{eq}} + \Gamma_{13} |\Omega_c|^2 (1 - \sigma_{44}^{\text{eq}})}{X_2}, \\ \sigma_{22}^{(0)} &= \frac{\gamma [\Gamma_{3\gamma} X_1 + |\Omega_c|^2] \sigma_{22}^{\text{eq}}}{X_2}, \\ \sigma_{33}^{(0)} &= \frac{\gamma |\Omega_c|^2 \sigma_{22}^{\text{eq}}}{X_2}, \\ \sigma_{44}^{(0)} &= \frac{[\gamma \Gamma_{3\gamma} X_1 + (2\gamma + \Gamma_{13}) |\Omega_c|^2] \sigma_{44}^{\text{eq}} + \Gamma_{43} |\Omega_c|^2 (1 - \sigma_{11}^{\text{eq}})}{X_2}, \\ \sigma_{32}^{(0)} &= -\frac{\Omega_c}{d_{32}} \cdot \frac{\gamma \Gamma_{3\gamma} X_1 \sigma_{22}^{\text{eq}}}{X_2} \end{aligned} \quad (4)$$

and  $\sigma_{21}^{(0)} = \sigma_{31}^{(0)} = 0$ , where  $\Gamma_{3\gamma} \equiv \gamma + \Gamma_3$ ,  $X_1 \equiv \{[(\Delta_3 - \Delta_2) - k_c v]^2 + \gamma_{32}^2\}/(2\gamma_{32})$  and  $X_2 \equiv \gamma(\gamma + \Gamma_3)X_1 + (2\gamma + \Gamma_{13} + \Gamma_{43})|\Omega_c|^2$ . Note that in above expressions  $d_{21} = d_{21}(v) = -(k_p - k_c)v + \Delta_2 - \Delta_1 + i\gamma_{21}$ ,  $d_{31} = d_{31}(v) = -k_p v + \Delta_3 - \Delta_1 + i\gamma_{31}$ , and  $d_{32} = d_{32}(v) = -k_c v + \Delta_3 - \Delta_2 + i\gamma_{32}$ .

When switching on the probe field, the base state (4) will be modified. In linear theory,  $\Omega_p$  is taken as a very small quantity. At first order in  $\Omega_p$ , the populations and the coherence between the states  $|2\rangle$  and  $|3\rangle$  are not changed, but with

$$\begin{aligned}\Omega_p^{(1)} &= F e^{i\theta}, \\ \sigma_{21}^{(1)} &= -\frac{(\omega + d_{31})\sigma_{32}^{*(0)} + \Omega_c^*(\sigma_{11}^{(0)} - \sigma_{33}^{(0)})}{|\Omega_c|^2 - (\omega + d_{21})(\omega + d_{31})} F e^{i\theta} \\ &= a_{21}^{(1)} F e^{i\theta}, \\ \sigma_{31}^{(1)} &= \frac{(\omega + d_{21})(\sigma_{11}^{(0)} - \sigma_{33}^{(0)}) + \Omega_c\sigma_{32}^{*(0)}}{|\Omega_c|^2 - (\omega + d_{21})(\omega + d_{31})} F e^{i\theta} \\ &= a_{31}^{(1)} F e^{i\theta},\end{aligned}\tag{5}$$

where  $F$  is a constant,  $\theta = K(\omega)z - \omega t$ . The linear dispersion relation  $K(\omega)$  [25] is given by

$$K(\omega) = \frac{\omega}{c} + \kappa_{13} \int_{-\infty}^{\infty} dv f(v) \frac{(\omega + d_{21})(\sigma_{11}^{(0)} - \sigma_{33}^{(0)}) + \Omega_c\sigma_{32}^{*(0)}}{|\Omega_c|^2 - (\omega + d_{21})(\omega + d_{31})}.\tag{6}$$

In thermal equilibrium,  $f(v)$  is the Maxwellian velocity distribution function, i.e.  $f(v) = 1/(\sqrt{\pi} v_T) \exp[-v^2/v_T^2]$ , with  $v_T = \sqrt{2k_B T/M}$  the most probable speed at temperature  $T$ , and  $M$  the molecular mass. The integration in equation (6) with the Maxwellian distribution leads however to some complicated combination of error functions [26], which is very inconvenient for a simple and clear analytical approach. As did by Lee *et al.* [27], in the following we use the modified Lorentzian velocity distribution  $f(v) = v_T/[\sqrt{\pi}(v_T^2 + v^2)]$  to replace the Maxwellian distribution.

We are interested in two different cases: co-propagating configuration ( $k_p \approx k_c$ ) and counter-propagating configuration ( $k_p \approx -k_c$ ), discussed below separately.

### 3.2. Hot molecules with co-propagating configuration

In this configuration, one has  $d_{21} = \Delta_2 - \Delta_1 + i\gamma_{21}$ ,  $d_{31} = -k_p v + \Delta_3 - \Delta_1 + i\gamma_{31}$  and  $d_{32} = -k_p v + \Delta_3 - \Delta_2 + i\gamma_{32}$ . The second term on the right-hand side of equation (6) can be calculated by using residue theorem [28]. There are two poles in the lower half complex plane

$$k_p v = \Delta_3 - iX_3, \quad k_p v = -ik_p v_T,\tag{7}$$

with  $X_3 \equiv \{\gamma_{32}^2 + 2\gamma_{32}(2\gamma + \Gamma_{13} + \Gamma_{43})|\Omega_c|^2/[\gamma(\gamma + \Gamma_3)]\}^{1/2}$ . By taking a contour consisting of real axis and a semi-circle in the lower half complex plane [see the curves with arrows shown in figure 2(a)], we can calculate the integration in equation (6) analytically by just calculating the residues corresponding to the two poles, and obtain exact result

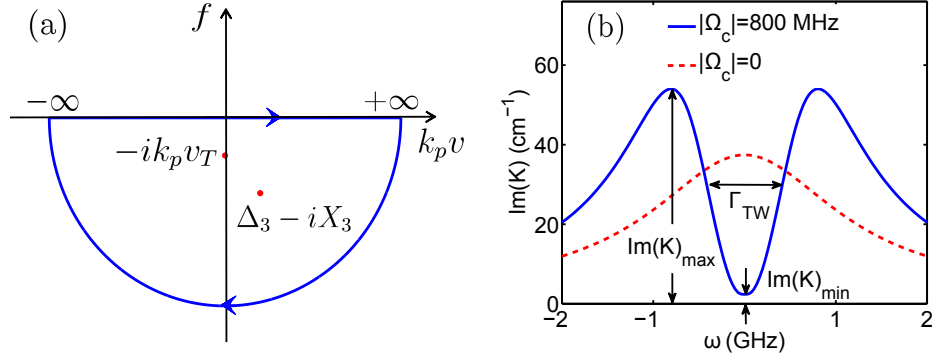


**Figure 2.** (Color online) (a): Two poles  $(\Delta_2, -iX_3)$ ,  $(0, -ik_p v_T)$  of the integrand in equation (6) in the lower half complex plane. The closed curve with arrows is the contour chosen for calculating the integration in equation (6) by using residue theorem. (b): Absorption spectrum  $\text{Im}(K)$  as a function of  $\omega$  for the hot molecular system. The solid (dashed) line for  $|\Omega_c| = 800$  MHz ( $|\Omega_c| = 0$ ). Definitions of  $\text{Im}(K)_{\min}$ ,  $\text{Im}(K)_{\max}$ , and the width of transparency window  $\Gamma_{\text{TW}}$  are indicated in the figure.

for the integration. Since the expression is lengthy, we just write down the one with  $\Delta_2 = \Delta_3 = 0$ ,  $\Delta\omega_D \gg \gamma_{jl}$ ,  $\gamma$ :

$$K = \frac{\omega}{c} + \mathcal{K}_1 + \mathcal{K}_2, \quad (8)$$

$$\mathcal{K}_1 = \frac{\sqrt{\pi}\kappa_{13}\Delta\omega_D[2\gamma_{32}(\omega + i\gamma_{21})A(-iX_3) - iX_3B]}{\gamma\Gamma_{3\gamma}(\Delta\omega_D^2 - X_3^2)X_3[|\Omega_c|^2 - (\omega + i\gamma_{21})(\omega + iX_3)]},$$

$$\mathcal{K}_2 = \frac{\sqrt{\pi}\kappa_{13}[2\gamma_{32}(\omega + i\gamma_{21})A(-i\Delta\omega_D) - i\Delta\omega_D B]}{\gamma\Gamma_{3\gamma}(X_3^2 - \Delta\omega_D^2)[|\Omega_c|^2 - (\omega + i\gamma_{21})(\omega + i\Delta\omega_D)]},$$

where  $\Delta\omega_D = k_p v_T$  (Doppler width),  $A(k_p v) \equiv X_2\sigma_{11}^{(0)} - \gamma|\Omega_c|^2\sigma_{22}^{\text{eq}}$  and  $B \equiv \gamma\Gamma_{3\gamma}|\Omega_c|^2\sigma_{22}^{\text{eq}}$ . Note that  $\mathcal{K}_1$  ( $\mathcal{K}_2$ ) is contributed by the first (second) pole. For cold molecules the second pole in equation (7) does not exist, thus  $\mathcal{K}_2 = 0$ . However, for hot molecules one has  $\mathcal{K}_2 \neq 0$  due to Doppler effect, and hence the system may have very different quantum interference characters comparing with that of cold molecules.

In most cases,  $K(\omega)$  can be Taylor expanded around the center frequency of the probe field (corresponding to  $\omega = 0$ ), i.e.,  $K(\omega) = K_0 + K_1\omega + (1/2)K_2\omega^2 \dots$ , where  $K_j \equiv (\partial^j K / \partial \omega^j)_{\omega=0}$ . The coefficients  $K_0$  describes the phase shift (real part) and the absorption (imaginary part) per unit length and  $1/\text{Re}(K_1)$  and  $1/\text{Re}(K_2)$  represent the group velocity  $v_g$  and group-velocity dispersion, respectively.

**3.2.1. Transparency window of probe-field absorption spectrum.** Shown in figure 2(b) is  $\text{Im}(K)$  as a function of  $\omega$ . The dashed (solid) line is for  $|\Omega_c| = 0$  ( $|\Omega_c| = 800$  MHz). System parameters given by  $\Gamma_{13} = \Gamma_{23} = \Gamma_{43} = 1.77 \times 10^7 \text{ s}^{-1}$ ,  $\gamma = 0.47 \times 10^6 \text{ s}^{-1}$ ,  $\gamma_{ji}^{\text{col}} = 4 \times 10^6 \text{ s}^{-1}$ ,  $\Delta\omega_D = 1.22 \text{ GHz}$ ,  $\kappa_{13} = 5 \times 10^{10} \text{ cm}^{-1}\text{s}^{-1}$  and  $\sigma_{11}^{\text{eq}} = \sigma_{22}^{\text{eq}} = 0.5$ . One sees that the absorption spectrum of the probe field for  $|\Omega_c| = 0$  has only a single absorption peak. However, a transparency window opens for a  $|\Omega_c| = 800$  MHz. The minimum ( $\text{Im}(K)_{\min}$ ), maximum ( $\text{Im}(K)_{\max}$ ), and width of transparency window ( $\Gamma_{\text{TW}}$ )



are defined in the figure.

From equation (8), we obtain the minimum of  $\text{Im}(K)$  at  $\omega = 0$ :

$$\text{Im}(K)_{\min} \simeq \frac{\sqrt{\pi}\kappa_{13}}{\Delta\omega_D} \left( \frac{\sigma_{11}^{\text{eq}}}{1+x_1} - \frac{\sigma_{22}^{\text{eq}}}{1+x_1} \frac{1}{1+\sqrt{x}} \right), \quad (9)$$

where  $x \equiv |\Omega_c|^2\gamma_{31}/(\gamma\Delta\omega_D^2)$  and  $x_1 \equiv |\Omega_c|^2/(\gamma_{21}\Delta\omega_D)$  are two dimensionless parameters. It is interesting that the system has absorption and gain, reflected by the first and the second terms on the right hand side of equation (9). The gain is due to non-vanishing  $\gamma$  and  $\sigma_{22}^{\text{eq}}$ . Obviously, if  $x \gg 1$  and  $x_1 \gg 1$ , i.e.  $|\Omega_c|^2\gamma_{31} \gg \gamma\Delta\omega_D^2$  and  $|\Omega_c|^2 \gg \gamma_{21}\Delta\omega_D$ , one has  $\text{Im}(K)_{\min} \approx 0$ , i.e. a large and deep transparency widow in the absorption spectrum is opened. The inequalities can be taken as the EIT condition [16, 27] of the system. When  $\gamma_{21} \approx \gamma$ , this condition is simplified to  $|\Omega_c|^2\gamma_{31} \gg \gamma\Delta\omega_D^2$ .

Under the above condition, we obtain  $\text{Im}(K)_{\max} \simeq \kappa_{13}\sigma_{11}^{\text{eq}}\sqrt{\pi}/\Delta\omega_D$  located at  $\omega \approx \pm\Omega_c$ , and

$$\Gamma_{\text{TW}} \approx 2 \left[ \frac{2|\Omega_c|^2 + \Delta\omega_D^2 - \Delta\omega_D\sqrt{\Delta\omega_D^2 + 4|\Omega_c|^2}}{2} \right]^{1/2}. \quad (10)$$

*3.2.2. EIT-ATS crossover.* One of our main purposes is to explicitly analyze the detailed characters of quantum interference effect of the system, which can be done by extending the spectrum decomposition method introduced in [4, 5, 6, 7]. Note that  $\mathcal{K}_j$  ( $j = 1, 2$ ) in equation (8) can be decomposed as

$$\mathcal{K}_j = \eta_j \left( \frac{A_{j+}}{\omega - \delta_{j+}} + \frac{A_{j-}}{\omega - \delta_{j-}} \right), \quad (11)$$

where  $\eta_j$ ,  $A_{j\pm}$  are constants,  $\delta_{j+}$  and  $\delta_{j-}$  are two spectrum poles, all of which have been given explicitly in Appendix A. From equation (11) we can get explicit expressions of  $\text{Im}(\mathcal{K}_j)$  ( $j = 1, 2$ ). However, their general expressions are lengthy and complicated. In order to illustrate the quantum interference effect in a simple and clear way, we decompose  $\text{Im}(\mathcal{K}_j)$  according to different regions of  $\Omega_c$ .

(i). *Weak control field region* (i.e.  $|\Omega_c| < \Omega_{\text{ref}} \equiv \Delta\omega_D/2$ ): In this region, one has  $\text{Re}(\delta_{j\pm})=0$ ,  $\text{Im}(A_{j\pm})=0$ , we obtain

$$\begin{aligned} \text{Im}(K) &= \sum_{j=1}^2 \text{Im}(\mathcal{K}_j) = \sum_{j=1}^2 \eta_j \left( \frac{C_{j+}}{\omega^2 + W_{j+}^2} + \frac{C_{j-}}{\omega^2 + W_{j-}^2} \right) \\ &= L_1 + L_2, \end{aligned} \quad (12)$$

where  $L_1$  and  $L_2$  are defined by

$$\begin{aligned} L_1 &= \frac{\eta_1 C_{1-}}{\omega^2 + W_{1-}^2} + \frac{\eta_2 C_{2-}}{\omega^2 + W_{2-}^2}, \\ L_2 &= \frac{\eta_1 C_{1+}}{\omega^2 + W_{1+}^2} + \frac{\eta_2 C_{2+}}{\omega^2 + W_{2+}^2}, \end{aligned} \quad (13)$$



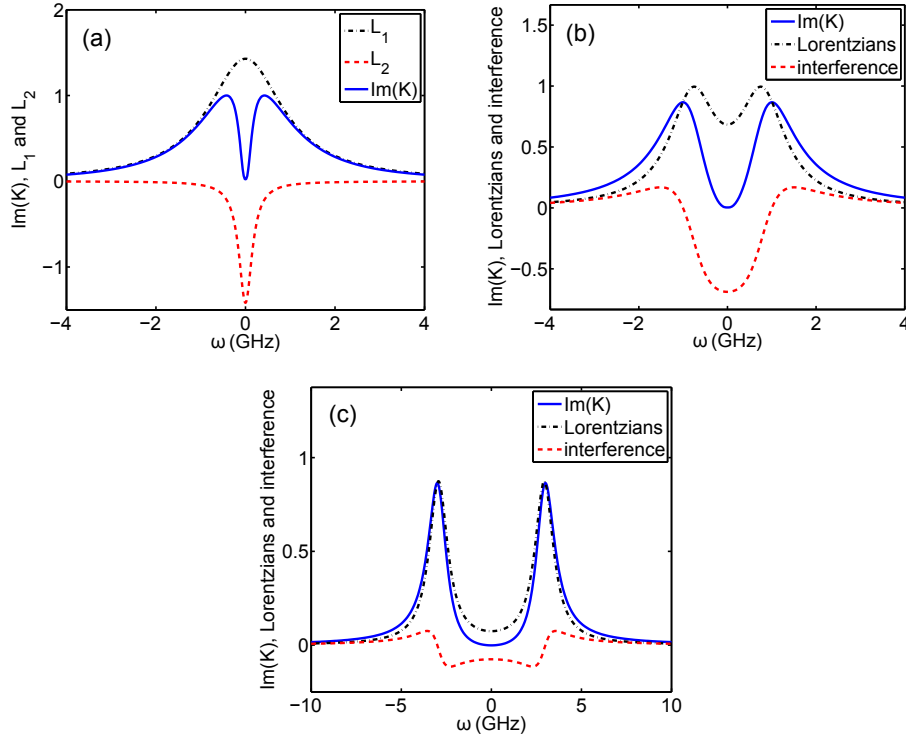


**Figure 3.** (Color online) EIT-ATS crossover for hot molecules in the co-propagating configuration. (a): Absorption spectrum in the region  $|\Omega_c| < \Omega_{\text{ref}} \equiv \Delta\omega_D/2$  contributed by positive  $L_1$  (dashed-dotted line), negative  $L_2$  (dashed line), and total absorption spectrum  $\text{Im}(K)$  (solid line). (b) and (c): Absorption spectrum by two Lorentzians (dashed-dotted line), destructive interference (dashed line), and total absorption spectrum  $\text{Im}(K)$  (solid line), in the region  $|\Omega_c| > \Omega_{\text{ref}}$  and  $|\Omega_c| \gg \Omega_{\text{ref}}$ , respectively. Panels (a), (b) and (c) correspond to EIT, EIT-ATS crossover, and ATS, respectively.

with real constants

$$\begin{aligned}
 C_{j+} &= -W_{j+}(W_{j+} + \Gamma_j^w)/(W_{j+} - W_{j-}), \\
 C_{j-} &= W_{j-}(W_{j-} + \Gamma_j^w)/(W_{j+} - W_{j-}), \\
 W_{1\pm} &= \frac{1}{2} \left[ X_3 + \gamma_{21} \pm \sqrt{(X_3 - \gamma_{21})^2 - 4|\Omega_c|^2} \right], \\
 W_{2\pm} &= \frac{1}{2} \left[ \Delta\omega_D + \gamma_{21} \pm \sqrt{(\Delta\omega_D - \gamma_{21})^2 - 4|\Omega_c|^2} \right], \\
 \Gamma_1^w &= \gamma_{21} - \frac{X_3 B}{2\gamma_{32} A(-iX_3)}, \\
 \Gamma_2^w &= \gamma_{21} - \frac{\Delta\omega_D B}{2\gamma_{32} A(-i\Delta\omega_D)}. \tag{14}
 \end{aligned}$$

Shown in figure 3(a) are results of  $L_1$ , which is a positive single peak (the dashed-dotted line), and  $L_2$ , which is a negative single peak (the dashed line). System parameters are given by  $\Gamma_{13} = \Gamma_{23} = \Gamma_{43} = 1.77 \times 10^7 \text{ s}^{-1}$ ,  $\gamma = 0.47 \times 10^6 \text{ s}^{-1}$ ,  $\gamma_{jl}^{\text{col}} = 4 \times 10^6 \text{ s}^{-1}$ ,  $\Delta\omega_D = 1.22 \text{ GHz}$ , and  $\Omega_c = 414 \text{ MHz}$ . The sum of the positive  $L_1$  and negative  $L_2$  gives  $\text{Im}(K)$  (the solid line), which displays a absorption doublet

with a significant transparency window near at  $\omega = 0$ . Because there exists a *destructive* interference in the probe-field absorption spectrum, the phenomenon found here belongs to EIT according to the criterion given in [5, 6, 7].

(ii). *Intermediate control field region* (i.e.  $|\Omega_c| > \Omega_{\text{ref}}$ ): By extending the approach by Agarwal [4], we can decompose  $\text{Im}(\mathcal{K}_j)$  ( $j = 1, 2$ ) as

$$\begin{aligned} \text{Im}(\mathcal{K}_j) = \eta_j \left\{ \frac{1}{2} \left[ \frac{W_j}{(\omega - \delta_j^r)^2 + W_j^2} + \frac{W_j}{(\omega + \delta_j^r)^2 + W_j^2} \right] \right. \\ \left. + \frac{g_j}{2\delta_j^r} \left[ \frac{\omega - \delta_j^r}{(\omega - \delta_j^r)^2 + W_j^2} - \frac{\omega + \delta_j^r}{(\omega + \delta_j^r)^2 + W_j^2} \right] \right\}, \end{aligned} \quad (15)$$

where

$$\begin{aligned} W_1 &= (\gamma_{21} + X_3)/2, \\ W_2 &= (\gamma_{21} + \Delta\omega_D)/2, \\ \delta_1^r &= \sqrt{4|\Omega_c|^2 - (X_3 - \gamma_{21})^2}/2, \\ \delta_2^r &= \sqrt{4|\Omega_c|^2 - (\Delta\omega_D - \gamma_{21})^2}/2, \\ g_1 &= \frac{X_3 - \gamma_{21}}{2} + \frac{X_3 B}{2\gamma_{32}A(-iX_3)}, \\ g_2 &= \frac{\Delta\omega_D - \gamma_{21}}{2} + \frac{\Delta\omega_D B}{2\gamma_{32}A(-i\Delta\omega_D)}. \end{aligned} \quad (16)$$

The first two terms in the first square bracket on the right hand side of equation (15) are two Lorentzians, resulted from the absorption from two different pathways corresponding to the two dressed states created by the coupling field. The terms in the second square bracket are interference terms, the magnitudes of which are controlled by the parameter  $g_j$ . If  $g_j > 0$  ( $g_j < 0$ ) the interference is destructive (constructive).

Figure 3(b) shows the result of the probe-field absorption spectrum as functions of  $\omega$  for  $|\Omega_c| > \Omega_{\text{ref}}$ . The dashed-dotted line (dashed line) denotes the contribution by two Lorentzians (interference terms). We see that the interference is destructive. The solid line gives the result of  $\text{Im}(K)$ . System parameters used are the same as those in panel (a) but with  $\Omega_c = 1$  GHz. A transparency window opens due to the combined effect of EIT and ATS, which is deeper and wider than that in panel (a). We call such phenomenon as EIT-ATS crossover.

(iii). *Large control field region* (i.e.  $|\Omega_c| \gg \Omega_{\text{ref}}$ ): In this case, the quantum interference strength  $g_j/\delta_j^r$  in equation (15) is very weak and negligible. We have

$$\text{Im}(\mathcal{K}_j) \approx \frac{\eta_j}{2} \left[ \frac{W_j}{(\omega - \delta_j^r)^2 + W_j^2} + \frac{W_j}{(\omega + \delta_j^r)^2 + W_j^2} \right], \quad (17)$$

being to a sum of two Lorentzians.

Shown in the panel (c) of figure 3 is the result of the probe-field absorption spectrum as functions of  $\omega$  for  $|\Omega_c| \gg \Omega_{\text{ref}}$ . The dashed-dotted line represents the contribution by the sum of the two Lorentzians. For illustration, we have also plotted the contribution from the small interference terms [neglected in equation (17)], denoted by the dashed line. We see that the interference is still destructive but very small. The solid line is the

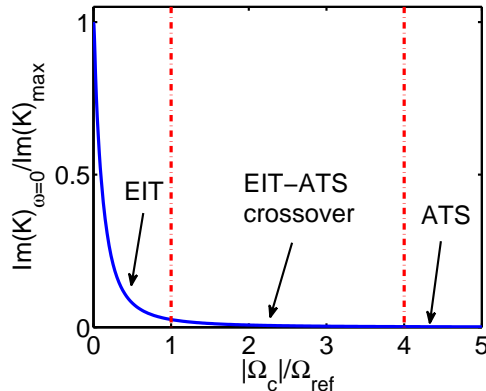


**Figure 4.** (Color online) The “phase diagram” illustrating the transition from EIT to ATS for hot molecules in the co-propagating configuration. Shown is  $\text{Im}(K)_{\omega=0}/\text{Im}(K)_{\max}$  as a function of  $|\Omega_c|/\Omega_{\text{ref}}$ . Three regions (EIT, EIT-ATS crossover, and ATS) are divided by two dash-dotted lines.

curve of  $\text{Im}(K)$ , which has two resonances at  $\omega \approx \pm\Omega_c$ . Parameters used are the same as those in panel (a) and (b) but with  $\Omega_c = 3$  GHz. Obviously, the phenomenon found in this situation belongs to ATS because the transparency window opened is mainly due to the contribution of the two Lorentzians.

From above results, we see that the probe-field absorption spectrum experiences a transition from EIT to ATS as  $\Omega_c$  is changed from weak to strong values. Since in three-level systems such phenomenon happens quite often and is universal, we divide quantum interference effects into three classes, i.e. the EIT region ( $|\Omega_c| < \Omega_{\text{ref}}$ ), the region of the EIT-ATS crossover ( $1 < |\Omega_c|/\Omega_{\text{ref}} \leq 4$ ), and ATS region ( $|\Omega_c|/\Omega_{\text{ref}} > 4$ ). Figure 4 shows a “phase diagram” that illustrates the transition from the EIT to ATS by plotting  $\text{Im}(K)_{\omega=0}/\text{Im}(K)_{\max}$  as a function of  $|\Omega_c|/\Omega_{\text{ref}}$ . Note that we have defined  $\text{Im}(K)_{\omega=0}/\text{Im}(K)_{\max} = 0.01$  as the border between EIT-ATS crossover and ATS regions.

*3.2.3. Comparison with experiment.* To check the theoretical prediction given above, it is necessary to make a comparison with the experiment reported recently by Lazoudis *et al.* [9], which was performed with a co-propagating configuration. Using system parameters  $\Gamma_{13} = \Gamma_{23} = \Gamma_{43} = 1.77 \times 10^7 \text{ s}^{-1}$ ,  $\gamma = 0.47 \text{ MHz}$ ,  $\gamma_{jl}^{\text{col}} = 4 \text{ MHz}$ , and  $\Delta\omega_D = 1.22 \text{ GHz}$ , we have calculated probe-field absorption spectrum  $\text{Im}(K)$  as a function of frequency  $\omega$ , with  $\Omega_c = 414 \text{ MHz}$  (EIT region) and the control-field detuning  $-55 \text{ MHz}$ . The result is plotted as the dashed line of figure 5, which agrees fairly with the experimental one (the solid line) measured in [9] (see figure 5(a) of [9]). Note that here we have plotted the quantity  $\text{Im}(K)$ , which is proportional to fluorescence intensity (measured in [9]) related to the state  $|3\rangle$  because  $\sigma_{33} \simeq 2|\Omega_p|^2\text{Im}(K)/(\gamma + \Gamma_3)$  [29]. The small difference for depth and width of the EIT dip between our result and the experiment is due to the approximation by using the modified Lorentzian distribution to replace the Maxwellian velocity distribution.

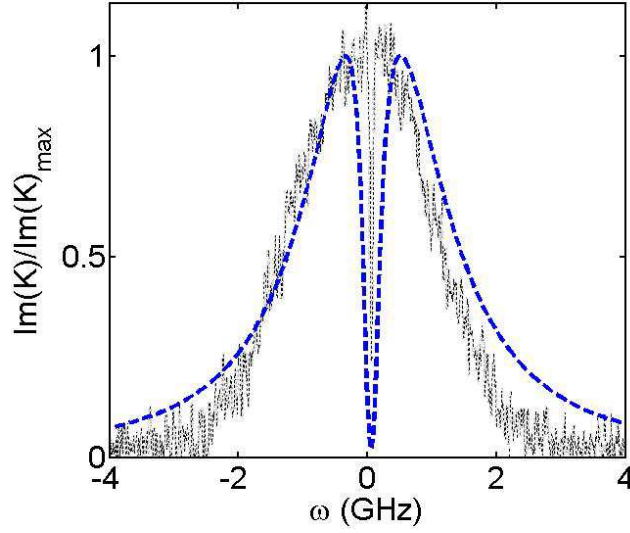


**Figure 5.** (Color online) Probe-field absorption spectrum  $\text{Im}(K)/\text{Im}(K)_{\max}$  as a function of frequency  $\omega$ , with  $\Omega_c = 414$  MHz (EIT region). The dashed line is theoretical result. The solid line is the experimental one reported in Ref. [9].

### 3.3. Hot molecules with counter-propagating configuration

We now move to the situation when the probe and control fields are arranged as a counter-propagating configuration. Here,  $d_{21} = \Delta_2 - \Delta_1 - 2k_p v + i\gamma_{21}$  and  $d_{32} = \Delta_3 - \Delta_2 + k_p v + i\gamma_{32}$ . Then we obtain

$$K = \frac{\omega}{c} + \frac{\kappa_{13}}{\gamma\Gamma_{3\gamma}}(\mathcal{K}_1 + \mathcal{K}_2), \quad (18)$$

$$\mathcal{K}_1 = \frac{\sqrt{\pi}\Delta\omega_D[2\gamma_{32}(\omega + i2X_3)A(-iX_3) + iX_3B]}{(\Delta\omega_D^2 - X_3^2)X_3[|\Omega_c|^2 - (\omega + 2iX_3)(\omega + iX_3)]},$$

$$\mathcal{K}_2 = \frac{\sqrt{\pi}[2\gamma_{32}(\omega + i2\Delta\omega_D)A(-i\Delta\omega_D) + i\Delta\omega_D B]}{(X_3^2 - \Delta\omega_D^2)[|\Omega_c|^2 - (\omega + i2\Delta\omega_D)(\omega + i\Delta\omega_D)]},$$

where  $\mathcal{K}_1$  and  $\mathcal{K}_2$  are obtained from the poles  $k_p v = \Delta_3 - iX_3$  and  $k_p v = -ik_p v_T$ , respectively.

We have carried out a similar spectrum decomposition as that did for the co-propagating configuration given above. For saving space, here we omit concrete expressions of the spectrum decomposition but present probe-field absorption spectra in three typical control-field regions in figure 6.

Shown in the panel (a) of figure 6 is the result of probe-field absorption spectrum  $\text{Im}(K)$  in weak control-field region (i.e.  $|\Omega_c| < \Omega_{\text{ref}}$ ) as a function of  $\omega$  for  $\Omega_c = 500$  MHz. As in figure 3(a),  $\text{Im}(K)$  is also the sum of two terms, i.e.  $L_1$  and  $L_2$ . Nevertheless, now both  $L_1$  and  $L_2$  are positive, as illustrated by the dashed-dotted line and dashed line, respectively. We see that  $\text{Im}(K)$  (the solid line) displays only a positive single peak, there is no transparency window, and the reason is that the quantum interference becomes constructive (the red dashed line) for the counter-propagating configuration. Thus,

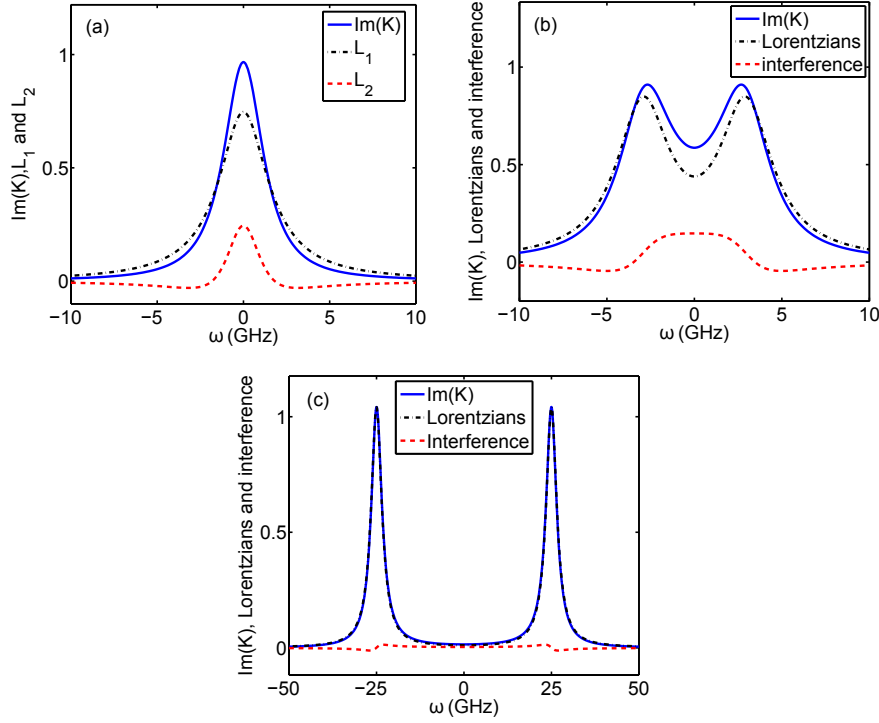


**Figure 6.** (Color online) Probe-field absorption spectrum for hot molecules in the counter-propagating configuration. (a): Absorption spectrum in the region  $|\Omega_c| < \Omega_{\text{ref}} \equiv \Delta\omega_D/2$  contributed by positive  $L_1$  (dashed-dotted line) and  $L_2$  (dashed line), and total absorption spectrum  $\text{Im}(K)$  (solid line). (b) and (c): Absorption spectrum by two Lorentzians (dashed-dotted line), constructive interference (dashed line), and total absorption spectrum  $\text{Im}(K)$  (solid line), in the region  $|\Omega_c| > \Omega_{\text{ref}}$  and  $|\Omega_c| \gg \Omega_{\text{ref}}$ , respectively.

different from the case of the co-propagating configuration, in weak control-field region an EIT which we have defined as transparency window plus a destructive interference does not exist.

Shown in figure 6(b) and (c) are results of the probe-field absorption spectra as functions of  $\omega$  for  $|\Omega_c| > \Omega_{\text{ref}}$  and  $|\Omega_c| \gg \Omega_{\text{ref}}$ , respectively. System parameters are given by  $\Gamma_{13} = \Gamma_{23} = \Gamma_{43} = 1.77 \times 10^7 \text{ s}^{-1}$ ,  $\gamma = 0.47 \times 10^6 \text{ s}^{-1}$ ,  $\gamma_{ij}^{\text{col}} = 4 \times 10^6 \text{ s}^{-1}$ , and  $\Delta\omega_D = 1.22 \text{ GHz}$ , with  $\Omega_c = 3 \text{ GHz}$  (in the intermediate control-field region) and  $\Omega_c = 25 \text{ GHz}$  (in the large control-field region) for the panel (b) and the panel (c), respectively. The dashed-dotted line (dashed line) denotes the contribution by the sum of two Lorentzians terms (interference terms) in  $\text{Im}(K)$ . The solid line gives the result of  $\text{Im}(K)$ . We see that the interferences near the probe-field center frequency (i.e.  $\omega = 0$ ) are always constructive. Consequently, different from the case of the co-propagating configuration, no EIT-ATS crossover happens.

Shown in figure 7 is the “phase diagram” that illustrates the transition from the constructive interference to ATS for the counter-propagating configuration by plotting  $\text{Im}(K)_{\omega=0}/\text{Im}(K)_{\text{max}}$  as a function of  $|\Omega_c|/\Omega_{\text{ref}}$ . Three regions are divided as constructive interference, ATS with constructive interference, and ATS, respectively.

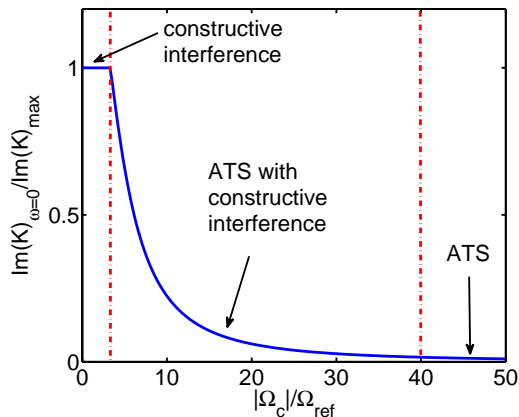


**Figure 7.** (Color online)  $\text{Im}(K)_{\omega=0}/\text{Im}(K)_{\max}$  as the function of the control field  $|\Omega_c|/\Omega_{\text{ref}}$  for hot molecules in the counter-propagating configuration. Three regions (constructive interference, ATS with constructive interference and ATS) are divided by two dashed-dotted lines.

### 3.4. Cold molecules and comparison for various cases

Our model presented in section 2 is also valid for cold molecules. In this case, one should take  $v = 0$  in the Bloch equation (2), and  $f(v) = \delta(v)$  in the Maxwell equation (3). The solutions (4) and (5) are still valid but one must take  $v = 0$  there. However, the dispersion relation (6) is replaced by

$$K(\omega) = \frac{\omega}{c} + \frac{\kappa_{13}(\sigma_{11}^{(0)} - \sigma_{33}^{(0)})(\omega + i\Gamma)}{|\Omega_c|^2 - (\omega + i\gamma_{21})(\omega + i\gamma_{31})}, \quad (19)$$

with  $\Gamma = \gamma_{21} + |\Omega_c|^2(\sigma_{33}^{(0)} - \sigma_{22}^{(0)})/[\gamma_{32}(\sigma_{11}^{(0)} - \sigma_{33}^{(0)})]$ . Here  $\Delta_2 = \Delta_3 = 0$  has been taken for simplicity.

A similar spectrum decomposition can be done like that did for hot molecules, which is omitted here. Shown in figure 8 is the probe-field absorption spectrum  $\text{Im}(K)_{\omega=0}/\text{Im}(K)_{\max}$  as a function of the control field  $|\Omega_c|/\Omega_{\text{ref}}$ , where  $\Omega_{\text{ref}} \equiv |\gamma_{21} - \gamma_{31}|/2$ . System parameters are given by  $\Gamma_{13} = \Gamma_{23} = \Gamma_{43} = 1.77 \times 10^7 \text{ s}^{-1}$ ,  $\gamma_{ij}^{\text{col}} = 1 \times 10^3 \text{ s}^{-1}$  and  $\sigma_{11}^{\text{eq}} = 1$ . From the figure, we obtain the similar conclusion as that obtained for co-propagation configuration, i.e. the probe-field absorption spectrum experiences also a transition from EIT to ATS as  $\Omega_c$  is increased. The quantum interference effect in the system can be divided into three regions, i.e. the EIT region ( $|\Omega_c| < \Omega_{\text{ref}}$ ), the region of the EIT-ATS crossover ( $1 < |\Omega_c|/\Omega_{\text{ref}} \leq 5$ ), and ATS region ( $|\Omega_c|/\Omega_{\text{ref}} > 5$ ).

From the results given above, we see that the quantum coherence in the open  $\Lambda$ -type molecular system has very interesting features, depending on the existence or non-existence of the Doppler broadening, and also depending on the beam propagating (co-propagating or counter-propagating) configurations. For comparison, in Table 1 some useful physical quantities, including EIT condition, absorption spectrum  $\text{Im}(K)|_{\omega=0}$ , group velocity  $v_g$ , and width of transparency window  $\Gamma_{\text{TW}}$ , are presented for several different physical cases.

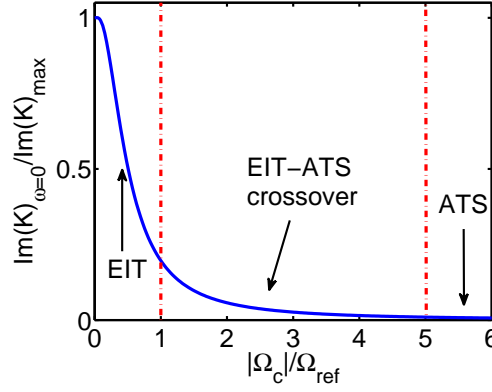


**Figure 8.** (Color online) Transition from EIT to ATS for cold molecules. Shown is  $\text{Im}(K)|_{\omega=0}/\text{Im}(K)_{\max}$  as a function of  $|\Omega_c|/\Omega_{\text{ref}}$ , where  $\Omega_{\text{ref}} \equiv |\gamma_{21} - \gamma_{31}|/2$ . Three regions (EIT, EIT-ATS crossover and ATS) are divided by two dash-dotted lines.

**Table 1.** Propagating properties of the probe field for various open  $\Lambda$ -type molecular systems, including EIT condition, absorption spectrum  $\text{Im}(K)|_{\omega=0}$ , width of transparency window  $\Gamma_{\text{TW}}$ , and group velocity  $v_g$  for three different cases. Other quantities appeared in the Table have been defined in the text. Mol.=Molecules, Co-prop.=Co-propagating configuration, Cou.-prop.=Counter-propagating configuration.

System	EIT condition	$\text{Im}(K) _{\omega=0}$	$\Gamma_{\text{TW}}$	$v_g$
Hot Mol. (Co-prop.)	$\frac{\gamma\Delta\omega_D^2}{\gamma_{31}} \leq  \Omega_c ^2 \leq \frac{(\Delta\omega_D)^2}{4}$	$\frac{\sqrt{\pi}\kappa_{13}\gamma_{21}}{ \Omega_c ^2}$	$\frac{2 \Omega_c ^2}{\Delta\omega_D}$	$\frac{ \Omega_c ^2}{\sqrt{\pi}\kappa_{13}}$
Hot Mol. (Cou.-prop.)	no EIT	$\frac{\sqrt{\pi}\kappa_{13}\Delta\omega_D}{ \Omega_c ^2}$	$2 \Omega_c  - \Delta\omega_D$	$\frac{ \Omega_c ^2}{\sqrt{\pi}\kappa_{13}}$
Cold Mol.	$\gamma_{21}\gamma_{31} \leq  \Omega_c ^2 \leq \frac{\gamma_{31}^2}{4}$	$\frac{\kappa_{13}\gamma_{21}}{ \Omega_c ^2}$	$\frac{2 \Omega_c ^2}{\gamma_{31}}$	$\frac{ \Omega_c ^2}{\kappa_{13}}$

The first line in the Table is for hot molecules working in the co-propagating configuration; the second line is for hot molecules working in the counter-propagating configuration; the third line is for cold molecules. There are EIT, EIT-ATS crossover, and ATS for both cold molecules and the hot molecules with the co-propagating configuration. But there is no EIT and no EIT-ATS crossover for the hot molecules with the counter-propagating configuration. Experimentally, up to now only the EIT in the co-propagating configuration has been demonstrated recently by experiment [9].

#### 4. Nonlinear pulse propagation

The theoretical approach given in the last two sections is valid not only for continuous-wave but also for pulsed probe fields. However, if the probe field is pulsed and has a larger amplitude, nonlinear effect induced by Kerr nonlinearity inherent in the system must taken into account. We stress that the theoretical scheme proposed in the present work is very suitable for the study of pulse propagation in multi-level systems.

In this section, we investigate nonlinear pulse propagation, especially ultraslow



optical solitons, in the present open hot molecular system with co-propagating configuration by using the method of multiple-scales. For this aim, we take the asymptotic expansion  $\sigma_{jl} - \sigma_{jl}^{(0)} = \sum_{m=1,2,\dots} \epsilon^m \sigma_{jl}^{(m)}$ ,  $\Omega_p = \sum_{m=1,2,\dots} \epsilon^m \Omega_p^{(m)}$ , with  $\sigma_{jj}^{(1)} = 0$  and  $\sigma_{32}^{(1)} = 0$ , where  $\epsilon$  is a small parameter denoting the typical amplitude of  $\Omega_p$  and all quantities on the right hand side of the asymptotic expansion are considered as functions of the multi-scale variables  $z_m = \epsilon^m z$  ( $m = 0, 1, 2$ ),  $t_m = \epsilon^m t$  ( $m = 0, 1$ ). Substituting the expansion into the MB equations (2) and (3), we obtain a series of linear but inhomogeneous equations for  $\sigma_{ij}^{(m)}$  and  $\Omega_p^{(m)}$  ( $m = 1-4$ ), which can be solved order by order.

The zeroth-order ( $m = 0$ ) and the first-order ( $m = 1$ ) solutions are the same as that given respectively by equation (4) and (5), by now  $\theta = K(\omega)z_0 - \omega t_0$  and  $F$  is yet to be determined envelope function of the ‘‘slow’’ variables  $t_1$ ,  $z_1$  and  $z_2$ . In the second order ( $m = 2$ ), a divergence-free solution for  $\Omega_p^{(2)}$  requires the solvability condition  $i[\partial F/\partial z_1 + (\partial K/\partial \omega)\partial F/\partial t_1] = 0$ , which shows that the envelope function  $F$  travels with complex group velocity  $(\partial K/\partial \omega)^{-1}$ . Explicit expressions of the second order solution have been given in Appendix B.

In the third order ( $m = 3$ ), the Kerr nonlinearity of the system plays a role. A divergence-free solution for  $\Omega_p^{(3)}$  gives rise to the equation

$$i \frac{\partial F}{\partial z_2} - \frac{1}{2} \frac{\partial^2 K}{\partial \omega^2} \frac{\partial^2 F}{\partial t_1^2} - W|F|^2 F e^{-2\bar{\alpha}z_2} = 0, \quad (20)$$

where  $\alpha = \text{Im}(K) = \epsilon^2 \bar{\alpha}$  and

$$W = -\kappa_{13} \int_{-\infty}^{\infty} dv f(v) \frac{\Omega_c a_{32}^{*(2)} + (\omega + d_{21})(a_{11}^{(2)} - a_{33}^{(2)})}{|\Omega_c|^2 - (\omega + d_{21})(\omega + d_{31})}, \quad (21)$$

with coefficients  $a_{11}^{(2)}$ ,  $a_{22}^{(2)}$  and  $a_{32}^{(2)}$  are defined in Appendix B.

Combining equation (20) and the solvability condition in the second order, we obtain

$$i \frac{\partial}{\partial z} U - \frac{1}{2} \frac{\partial^2 K}{\partial \omega^2} \frac{\partial^2 U}{\partial \tau^2} - W|U|^2 U e^{-2\alpha z} = 0, \quad (22)$$

where  $\tau = t - z/v_g$  and  $U = \epsilon F$ . Equation (22) is a nonlinear Schrödinger (NLS) equation describing time evolution of the envelope function  $F$ , in which  $W$  is proportional to third-order nonlinear susceptibility (Kerr coefficient) relevant to self-phase modulation, which is necessary for the formation of a shape-preserved probe pulse.

The key for the formation and propagation of an optical soliton in the system requires two conditions. The first is a balance between dispersion and nonlinearity, and the second is the absorption of the probe field must be negligibly small. Generally, the coefficients of the equation (22) are complex, which means that a soliton, even if it is produced initially, may be highly unstable during propagation. However, as shown below, a realistic set of system parameters can be found under the EIT condition so that the imaginary part of these coefficients can be made much smaller than their corresponding real part. Thus it is possible to get a shape-preserving nonlinear localized solution that can propagate a rather long distance without a significant distortion.

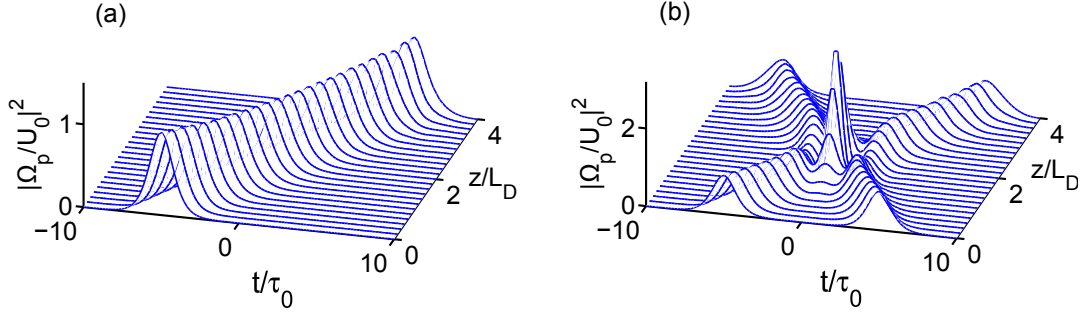


**Figure 9.** (Color online) (a): Ultraslow optical solitons and their interaction in the hot molecular system. (a): Three-dimensional plot of the waveshape of  $|\Omega_p/U_0|^2$  as a function of  $z/L_D$  and  $t/\tau_0$ . (b): Collision between two ultraslow optical solitons.

Neglecting the small imaginary part of the coefficients and taking  $\omega = 0$ , equation (22) can be written into the dimensionless form  $i\partial u/\partial s + \partial^2 u/\partial \sigma^2 + 2|u|^2 u = 0$ , with  $s = -z/(2L_D)$ ,  $\sigma = \tau/\tau_0$ , and  $u = U/U_0$ . Here  $\tau_0$  is typical pulse duration,  $L_D = \tau_0^2/\tilde{K}_2$  is typical dispersion length, and  $U_0 = (1/\tau_0)\sqrt{\tilde{K}_2/\tilde{W}}$  is typical half Rabi frequency of the probe field, with  $\tilde{K}_2$  and  $\tilde{W}$  being the real part of  $K_2 = (\partial^2 K/\partial \omega^2)_{\omega=0}$  and  $W|_{\omega=0}$ , respectively. Then one can obtain various soliton solutions for  $u$ . A single-soliton solution in terms of the half Rabi frequency reads

$$\Omega_p = \frac{1}{\tau_0} \sqrt{\frac{\tilde{K}_2}{\tilde{W}}} \operatorname{sech} \left( \frac{t}{\tau_0} - \frac{z}{\tau_0 v_g} \right) \exp \left[ i \left( \tilde{K}_0 + \frac{1}{2L_D} \right) z \right] \quad (23)$$

with  $\tilde{K}_0 = \operatorname{Re}(K)|_{\omega=0}$ , which describes a bright soliton traveling with the propagating velocity  $v_g = [\operatorname{Re}(\partial K/\partial \omega)]^{-1}|_{\omega=0}$ .

We now give a realistic parameter set for the formation of the optical soliton given above. For a hot  $\text{Li}_2$  molecular gas, we choose  $\Omega_c = 600$  MHz,  $\Delta_2 = \Delta_3 \approx 2.36 \times 10^7$  s $^{-1}$ ,  $\tau_0 = 1.0 \times 10^{-7}$  s,  $\omega_p = 4.46 \times 10^{14}$  s $^{-1}$ , and other parameters are the same as those given in the previous text. Then we obtain  $K_2 = (5.51 + 0.672i) \times 10^{-16}$  cm $^{-1}$ s $^2$  and  $W = (1.75 + 0.298i) \times 10^{-16}$  cm $^{-1}$ s $^2$ ,  $L_D = L_{NL} = 18.2$  cm, and  $U_0 = 1.77 \times 10^7$  s $^{-1}$ . One sees that the imaginary part of  $K_2$  and  $W$  is indeed much smaller than their corresponding real part. The reason of so small imaginary part is due to the quantum interference effect contributed by the control field.

The propagating velocity of the probe pulse can be estimated by the real part of the linear dispersion relation (6). At the probe-field center frequency (i.e.  $\omega = 0$ ) we obtain  $v_g = [\operatorname{Re}(\partial K/\partial \omega)|_{\omega=0}]^{-1} \approx 2.13 \times 10^{-4}c$ . Consequently, the optical soliton obtained may travel with an ultraslow propagating velocity in the system.

The stability of the ultraslow optical soliton described above can be checked by using numerical simulations. In figure 9(a), we show the wave shape of  $|\Omega_p/U_0|^2$  as a function of  $z/L_D$  and  $t/\tau_0$ . The solution is obtained by numerically solving Eq. (22) with full complex coefficients included. The initial condition is given by  $\Omega_p(0, t) = U_0 \operatorname{sech}(t/\tau_0)$ . We see that the amplitude of the soliton undergoes only a slight decrease and its width

undergoes a slight increase due to the influence of the imaginary part of the coefficients. A simulation of the interaction between two ultraslow optical solitons is also carried out by inputting two identical solitons [see figure 9 (b)]. The initial condition is  $\Omega_p(0, t) = U_0 \text{sech}(t/\tau_0 - 5) + U_0 \text{sech}(t/\tau_0 + 5)$ . As time goes on, they collide, pass through, and depart from each other. The two solitons recover their initial waveforms after the collision. However, a phase shift is observed after the collision.

## 5. CONCLUSION

We have developed a systematic analytical approach on linear and nonlinear pulse propagations in an open  $\Lambda$ -type molecular system with Doppler broadening. In linear case, by using residue theorem and spectrum decomposition method, we have proved that there exists a crossover from EIT to ATS for the co-propagating configuration. However, there is no EIT and hence no EIT-ATS crossover for the counter-propagating configuration. We have provided various explicit formulas, including probe-field spectrum decomposition, EIT condition, and width of EIT transparency window, as well as a comparison with the result of cold molecules. Our analytical result agrees well with the experimental one reported recently by Lazoudis *et al* [9]. In nonlinear case, by using the method of multiple-scales, we have derived a nonlinear envelope equation for probe-field propagation. We show that stable ultraslow solitons can be realized in the open molecular system. New theoretical predictions presented in this work are helpful for guiding new experimental findings in coherent molecular systems and may have promising practical applications in coherent molecular spectroscopy, precision measurement, molecular quantum state control, nonlinear pulse propagation, and so on.

## Acknowledgments

This work was supported by NSF-China under Grant Numbers 10874043 and 11174080.

## Appendix A. Expressions of $\eta_j$ , $A_{j\pm}$ , and $\delta_{j\pm}$

$$\eta_1 = \frac{\kappa_{13}\sqrt{\pi}\gamma_{32}\Delta\omega_D A(-iX_3)}{\gamma\Gamma_{3\gamma}X_3(\Delta\omega_D^2 - X_3^2)}, \quad (\text{A.1})$$

$$\eta_2 = \frac{\kappa_{13}\sqrt{\pi}\gamma_{32}A(-i\Delta\omega_D)}{\gamma\Gamma_{3\gamma}(X_3^2 - \Delta\omega_D^2)}, \quad (\text{A.2})$$

$$\delta_{1\pm} = \frac{1}{2} \left[ -i(X_3 + \gamma_{21}) \pm \sqrt{4|\Omega_c|^2 - (X_3 - \gamma_{21})^2} \right], \quad (\text{A.3})$$

$$\delta_{2\pm} = \frac{1}{2} \left[ -i(\Delta\omega_D + \gamma_{21}) \pm \sqrt{4|\Omega_c|^2 - (\Delta\omega_D - \gamma_{21})^2} \right], \quad (\text{A.4})$$

$$A_{1\pm} = \mp \frac{\delta_{1\pm} - \left[ \gamma_{21} - \frac{X_3 B}{2\gamma_{32} A(-iX_3)} \right]}{\delta_{1+} - \delta_{1-}}, \quad (\text{A.5})$$

$$A_{2\pm} = \mp \frac{\delta_{2\pm} - \left[ \gamma_{21} - \frac{\Delta\omega_D B}{2\gamma_{32} A(-i\Delta\omega_D)} \right]}{\delta_{2+} - \delta_{2-}}. \quad (\text{A.6})$$

## Appendix B. Second-order solution of MB Equations

$$\begin{aligned} \sigma_{21}^{(2)} &= \frac{i}{D} [(\omega + d_{31})a_{21}^{(1)} - \Omega_c^* a_{31}^{(1)}] \frac{\partial F}{\partial t_1} e^{i\theta} \\ &= a_{21}^{(2)} \frac{\partial F}{\partial t_1} e^{i\theta}, \end{aligned} \quad (\text{B.1})$$

$$\begin{aligned} \sigma_{31}^{(2)} &= \frac{i}{D} [(\omega + d_{21})a_{31}^{(1)} - \Omega_c a_{21}^{(1)}] \frac{\partial F}{\partial t_1} e^{i\theta} \\ &= a_{31}^{(2)} \frac{\partial F}{\partial t_1} e^{i\theta}, \end{aligned} \quad (\text{B.2})$$

$$\begin{aligned} \sigma_{33}^{(2)} &= \frac{i}{D_1} \left\{ [\gamma^2(\omega + d_{32})(\omega + d_{32}^*) + 2\gamma\gamma_{32}|\Omega_c|^2] \right. \\ &\quad \times (a_{31}^{*(1)} - a_{31}^{(1)}) - \gamma(\gamma + \Gamma_{31}) \left[ \Omega_c a_{21}^{(1)}(\omega + d_{32}) \right. \\ &\quad \left. \left. - \Omega_c^* a_{21}^{*(1)}(\omega + d_{32}^*) \right] \right\} |F|^2 e^{-2\bar{\alpha}z_2} \\ &= a_{33}^{(2)} |F|^2 e^{-2\bar{\alpha}z_2}, \end{aligned} \quad (\text{B.3})$$

$$\begin{aligned} \sigma_{11}^{(2)} &= \left[ \frac{\Gamma_{13}}{\gamma + \Gamma_{31}} a_{33}^{(2)} - \frac{i}{\gamma + \Gamma_{31}} (a_{31}^{*(1)} - a_{31}^{(1)}) \right] |F|^2 e^{-2\bar{\alpha}z_2} \\ &= a_{11}^{(2)} |F|^2 e^{-2\bar{\alpha}z_2}, \end{aligned} \quad (\text{B.4})$$

$$\sigma_{22}^{(2)} = -(\sigma_{11}^{(2)} + \sigma_{33}^{(2)} + \sigma_{44}^{(2)}) = a_{22}^{(2)} |F|^2 e^{-2\bar{\alpha}z_2}, \quad (\text{B.5})$$

$$\sigma_{44}^{(2)} = \frac{\Gamma_{43}}{\gamma} a_{33}^{(2)} |F|^2 e^{-2\bar{\alpha}z_2} = a_{44}^{(2)} |F|^2 e^{-2\bar{\alpha}z_2}, \quad (\text{B.6})$$

$$\begin{aligned} \sigma_{32}^{(2)} &= \left[ \frac{\Omega_c}{\omega + d_{32}} (a_{33}^{(2)} - a_{22}^{(2)}) - \frac{a_{21}^{*(1)}}{\omega + d_{32}} \right] |F|^2 e^{-2\bar{\alpha}z_2} \\ &= a_{32}^{(2)} |F|^2 e^{-2\bar{\alpha}z_2}, \end{aligned} \quad (\text{B.7})$$

with  $D \equiv |\Omega_c|^2 - (\omega + d_{21})(\omega + d_{31})$  and  $D_1 \equiv \gamma[(\gamma + \Gamma_{23} + \Gamma_{43})(\gamma + \Gamma_{31}) + \gamma\Gamma_{13}](\omega + d_{32})(\omega + d_{32}^*) + 2\gamma_{32}[(2\gamma + \Gamma_{43})(\gamma + \Gamma_{31}) + \gamma\Gamma_{13}]|\Omega_c|^2$ .  $a_{21}^{(1)}$  and  $a_{31}^{(1)}$  have been defined in equation (5).

## References

- [1] Autler S R and Townes C R 1955 *Phys. Rev.* **100** 703
- [2] Fleischhauer M, Imamoglu A and Marangos J P 2005 *Rev. Mod. Phys.* **77** 633
- [3] Khurgin K B and Tucker R S (editors) 2009 *Slow Light: Science and Applications* (Boca Raton: CRC, Taylor and Francis)
- [4] Agarwal G S 1997 *Phys. Rev. A* **55** 2467

- [5] Anisimov P and Kocharovskaya O 2008 *J. Mo d. Opt.* **55** 3159
- [6] Abi-Salloum T Y 2010 *Phys. Rev. A* **81** 053836
- [7] Anisimov P M, Dowling J P and Sanders B C 2011 *Phys. Rev. Lett* **107** 163604
- [8] Qi J, Spano F C, Kirova T, Lazoudis A, Magnes J, Li L, Narducci L M, Field R W and Lyyra A M 2002 *Phys. Rev. Lett.* **88** 173003
- [9] Lazoudis A, Kirova T, Ahmed E H, Li L, Qi J and Lyyra A M 2010 *Phys. Rev. A.* **82** 023812
- [10] Li L, Qi P, Lazoudis A, Ahmed E and Lyyra A M 2005 *Chem. Phys. Lett.* **403** 262
- [11] Lazoudis A, Ahmed E H, Li L, Kirova T, Qi P, Hansson A, Magnes J and Lyyra A M 2008 *Phys. Rev. A* **78** 043405
- [12] Lazoudis A, Kirova T, Ahmed E H, Qi P, Huennekens J and Lyyra A M 2011 *Phys. Rev. A* **83** 063419
- [13] Ghosh S, Sharping J E, Ouzounov D G and Gaeta A L 2005 *Phys. Rev. Lett.* **94** 093902
- [14] Benabid F and Roberts P J 2011 *J. Mod. Opt.* **58** 87
- [15] Light P S, Benabid F, Pearce G J, Couny F and Bird D M 2009 *Appl. Phys. Lett.* **94** 141103
- [16] Li H, Chen H, Gubin M A, Rostovtsev Y V, Sautenkov V A and Scully M O 2010 *Laser Physics* **20** 1725
- [17] Hong T 2003 *Phys. Rev. Lett.* **90** 183901
- [18] Wu Y and Deng L 2004 *Phys. Rev. Lett.* **93** 143904
- [19] Huang G, Deng L and Payne M G 2005 *Phys. Rev. E* **72** 016617
- [20] Hang C, Huang G and Deng L 2006 *Phys. Rev. E* **73** 036607
- [21] Michinel H, Paz-Alonso M J and Perez-Garcia V M 2006 *Phys. Rev. Lett.* **96** 023903
- [22] Huang G, Hang C and Deng L 2008 *Phys. Rev. A* **77** 011803(R)
- [23] Yang W-X, Chen A-X, Si L-G, Jiang K, Yang X and Lee R-K 2010 *Phys. Rev. A* **81** 023814
- [24] Li L and Huang G 2010 *Phys. Rev. A* **82** 023809
- [25] The frequency and wavevector of the probe field are given by  $\omega_p + \omega$  and  $k_p + K(\omega)$ , respectively. Thus  $\omega = 0$  corresponds to the center frequency of the probe field
- [26] Ahmed E H and Lyyra A M 2007 *Phys. Rev. A* **76** 053407
- [27] Lee H, Rostovtsev Y, Bednar C J and Javan A 2003 *Appl. Phys. B* **76** 33-39
- [28] Byron F W and Fuller R W 1969 *Mathematics in Classical and Quantum Physics* vol. 2 (Addison-Wesley) Chap. 6
- [29] Figure 5(b)-(d) in [9] belong to results in the EIT region (i.e.  $\Omega_c < \Delta\omega_D/2$ ) measured for several values of small  $\Omega_c$ . In general, the smaller the  $\Omega_c$ , the narrower and shallower the EIT transparency window, which also agree with our theoretical calculation